DIGITAL PRODUCTIVITY AND OCEANS AND ATMOSPHERES FLAGSHIP
www.csiro.au

Hydrodynamic Modelling of Saline Inundation from Sea Level Rise in Kakadu National Park

James Hilton, Fletcher Woolard and Mahesh Prakash

Stage 2 Report

1st September 2014

Internal Client: Oceans and Atmospheres Flagship

CSIRO Digital Productivity Flagship

CSIRO Oceans and Atmospheres Flagship

Copyright and disclaimer

Important disclaimer

Contents

Figures

Tables

Acknowledgments

Funding bodies:

Oceans and Atmospheres Flagship

Executive summary

Kakadu National Park is a World Heritage Site in the Northern Territory. The freshwater floodplains and wetlands of the park support many of the bird, reptile and fish species found in Australia. Saltwater intrusion through potential sea level rise or cyclonic storm surges may impact these freshwater ecosystems. Effects of saltwater intrusion include loss of habitat for freshwater species, along with changes in traditional hunting and cultural heritage sites. In stage 1 of this project, the effects of potential sea level rise on Kakadu national park was examined and saltwater intrusion estimated from maximum inundation extents. In this stage of the project, phase 2, we apply a computational model to predict quantitative salinity values over inundated regions. An evapotranspiration model is used to ensure the correct prediction of deposition of salt on floodplains due to evaporation. In addition to sea level rise we also examine saltwater intrusion during storm surges caused by cyclones with associated heavy rainfall events. The scenarios investigated were for months in the wet season (March) and the dry season (October) using current day sea levels and a sea level rise of 70 cm. Additional wet season scenarios with a 3 meter storm surge were also carried out. The maximum area of saltwater intrusion was found to increase for both storm surges and sea level rise. However, heavy rainfall was found to potentially mitigate the effect of saltwater intrusion in upstream areas.

1 Introduction

Kakadu National Park (Fig. 1) is the largest and one of the most diverse national parks in Australia. The park is located within Arnhem land, at north eastern part of the Northern Territory, and runs from Van Diemen gulf in the north 200 km south to the escarpments of the Arnhem Land plateau. The northern part of the park is dominated by lowland floodplains, which are inundated by freshwater during the wet season, and the four major river systems: the East, South and West alligator rivers and the Wildman river. The park encompasses the entire catchment of the 160 km long South alligator river. One third of the bird species in Australia can be found in Kakadu, and the floodplains are the seasonal home to around 2.5 million waterbirds. The park is also home to one quarter of Australian freshwater and estuarine fish species as well as many species of small mammals and reptiles, including threatened species such as the saltwater crocodile (World Heritage Convention UNESCO, 2014).

Figure 1 - The Northern Territory and Van Diemen gulf, with Kakadu national park outlined in black.

The area has also been continuously inhabited by humans for over 40,000 years and the current Aboriginal people living in the region are part of the oldest surviving culture in the world. Both the ecological and cultural uniqueness of the park led to the addition of the park to the UNESCO World Heritage List, encompassing “all the natural and cultural attributes necessary to convey its outstanding universal value”. However, amongst the protection requirements for the site is a range of adaption and mitigation measures to manage the consequences of climate change in the region. Such consequences include potential sea level rise, changes in precipitation and changes in seasonal temperature ranges (Bayliss et al., 1997).

Saltwater intrusion of freshwater areas through sea level rise may result in the contraction of freshwater habitats and the spread of saline mudflats into vegetated areas. For the Kakadu wetlands this could lead to the loss of crocodile breeding grounds and magpie geese habitat, as well as affect the ability for the local people to gather food within these regions (Saynor et al. 2004). Saltwater intrusion on floodplains occurs through the expansion and creation of tidal creeks (Winn et al., 2006). A rapid expansion of a tidal creek network (30 km inland in 40 years) has been reported in the Mary river system, adjacent to Kakadu national park (Knighton et al. 1992). The high speed of the intrusion has been attributed to a number of factors, including the flat floodplains in the region and the high tidal ranges in the van Diemen gulf. The flat floodplains allow breaching of freshwater regions during exceptionally high tides which quickly form channels due to scouring action of the high tidal ranges (Bayliss et al., 1997). Additionally, feral buffalo form swim channels in the wet season, greatly accelerating the formation of tidal creeks.

This phase of the study investigates saltwater intrusion and mixing with freshwater regions using a hydrodynamic model. A key feature of the modelling done in the 2nd phase is that they are run over monthly periods in the dry (October) and wet (March) seasons. Tidal cycles, rainfall (during the wet season) and evaporation are taken into account. Additionally, the effect of cyclonic storm surges and associated heavy rainfall events are investigated in two of the scenarios. A set of scenarios with a sea level rise of 70 cm is also considered. As detailed in phase 1, 70 cm corresponds to a potential sea level rise for 2070 (BMT WBM, 2011). Metrics such as the maximum and median salinity and inundation extents are presented and discussed.

2 Methodology

The hydrodynamics were modelled using a conservative finite volume formulation of the shallow water equations. The shallow water equations are based on the assumption that the height of the water is much less than the width and length of the domain, allowing the vertical velocity to be depth averaged. This assumption allows the hydrodynamics to be reduced to a two-dimensional formulation, considerably simplifying the computational cost of modelling such systems. The depth-averaged assumption holds in this case as the tidal height is small in relation to the expanse of computational domain. The conservative shallow water equations are given by (Kurganov and Petrova, 2007):

$$\frac{\partial h}{\partial t} + \nabla \cdot \boldsymbol{q} = 0 \tag{1}$$

$$\frac{\partial \boldsymbol{q}}{\partial t} + \nabla(\boldsymbol{uq}) + \frac{1}{2} g \nabla h^2 + \boldsymbol{s} = 0 \tag{2}$$

$$\boldsymbol{s} = gh\,\nabla B + g n_m^2 h^{-\frac{7}{3}} |\boldsymbol{q}|^2\, \widehat{\boldsymbol{q}} \tag{3}$$

where h is the height of the water above the base level B, $\boldsymbol{q}$ is unit discharge given by $\boldsymbol{q} = h\boldsymbol{u}$, $\boldsymbol{u}$ is the horizontal velocity vector and g is gravity. The vector $\boldsymbol{s}$ combines a source term from the gradient of the base and a lossy drag term. The drag is based on a Manning drag formulation (Begnudelli and Sanders, 2007), where, n_m is the Manning drag coefficient.

Our computational formulation is based on a solution method presented by Kurganov and Petrova (2007). This method obeys both *well-balanced* and *positivity preserving* properties which are essential for realistic and stable shallow water simulations. The well-balanced property ensures that the numerical scheme does not perturb solutions which should remain stable, for example, a lake of water at rest. The positivity preserving property ensures that the height, h, remains positive everywhere. This is an especially difficult requirement to meet at interfaces between wet and dry regions within the simulation domain. Although such requirements appear conceptually straightforward, a scheme that meets both of these requirements is difficult to construct and has been the focus of much hydrodynamic research. The Kurganov and Petrova scheme uses a number of novel methodologies to ensure both of these essential properties are satisfied. These include a reformulation of the shallow water equations in terms of the total height above a given vertical

datum, local small-scale reconstruction of the input base topography to ensure a well-balanced solution and a modified linear reconstruction method for the water heights in the finite volume method. In our simulations we also include a minimum water height cut-off of 1 μm to prevent floating-point round-off error at very small water depths.

The salinity component was modelled using the depth averaged scalar advection-diffusion equation (Gross et al. 1999):

$$\frac{\partial(sh)}{\partial t} + \nabla \cdot (s\boldsymbol{q}) - \nabla(\varepsilon h \nabla s) = 0 \quad (4)$$

where *s* is the depth-averaged scalar concentration and ε is the diffusivity coefficient. Eq. (4) can be re-arranged using Eq. (1) to give:

$$h\frac{\partial s}{\partial t} + \boldsymbol{q} \cdot \nabla s - \nabla(\varepsilon h \nabla s) = 0 \quad (5)$$

In this study *s* was the depth averaged salinity value (in parts per thousand) and ε was set to be constant, based on an estimate of the maximum turbulent diffusion in the system. This was calculated as $\varepsilon \sim \frac{1}{6}\kappa h u^*$, where u^* is the shear velocity (Cea et al., 2007) and $u^* = u\sqrt{g}nh^{-\frac{1}{6}}$, so $\varepsilon \sim \frac{1}{6}\kappa q\sqrt{g}nh^{-\frac{1}{6}}$. Eq. (5) was solved using an explicit finite difference method.

The evapotranspiration component was modelled using the Penman-Monteith formulation. Due to the large number of unknown variables in the standard formulation, the FAO-56 model was used, which gave the rate of evapotranspiration from a fixed reference type of vegetation with a height of 0.12 m, a surface resistance of 70 s/m and an albedo value of 0.23 (Smith et al. 1992). Despite the use of a single vegetation type the model predicted values consistent with measured rates of approximately 6mm/day (Fig. 2). The Penman-Monteith equation used was:

$$R = \frac{0.408\Delta(R_n - G) + \gamma\left(\frac{900}{T + 273.3}\right)u_2 e_s\left(1 - \frac{R_h}{100}\right)}{\Delta + \gamma(1 + 0.34u_2)} \quad (6)$$

where Δ is the slope of the saturated pressure curve, R_n the net radiation flux (MJ m^{-2} day^{-1}), *G* the heat flux into the ground (MJ m^{-2} day^{-1}), calculated as $G = c_s R_n$, where c_s is the soil heat flux coefficient, γ is the psychrometric constant, estimated as $\gamma = 6.65\times10^{-4}P$, where *P* the atmospheric pressure (kPa), *T* is the mean air temperature (°C), u_2 the wind speed 2 m from the ground (m s^{-1}), e_s the mean saturated vapour pressure (kPa) and R_h the relative humidity (%). The slope of the saturated pressure curve, Δ, was calculated as:

$$\Delta = \frac{4098\left(0.6108e^{\left(\frac{17.27T_m}{T_m+273.3}\right)}\right)}{T_m + 273.3} \quad (7)$$

where T_m is the mean daily temperature. The mean saturated vapour pressure, e_s, was calculated as:

$$e_s = 0.6108e^{\left(\frac{17.27T}{T+273.3}\right)} \quad (8)$$

For the simulations in this study we used a constant Manning's drag of 0.015, corresponding to drag for light land usage which is consistent with the terrain in Kakadu National Park. The inputs required for the model are a base digital elevation model (DEM) of the topography and bathymetry for the region, the elevation of mean sea level and a tidal time series for boundary forcing. For the salinity component an initial distribution of salinity is required, which was approximated using the limiting behaviour in the wet and dry seasons. The diffusion coefficient ε was set to 0.1, based on a height O(10 m) and velocity O(10 m/s). For the evapotranspiration component, air temperature, wind speed, relative humidity and solar radiation time series inputs are required. The mean pressure used was 101.3 kPa and the mean temperature used in Eq. 7 was set to 20°C. The ground was assumed to be perfectly absorbing, with c_s = 0.

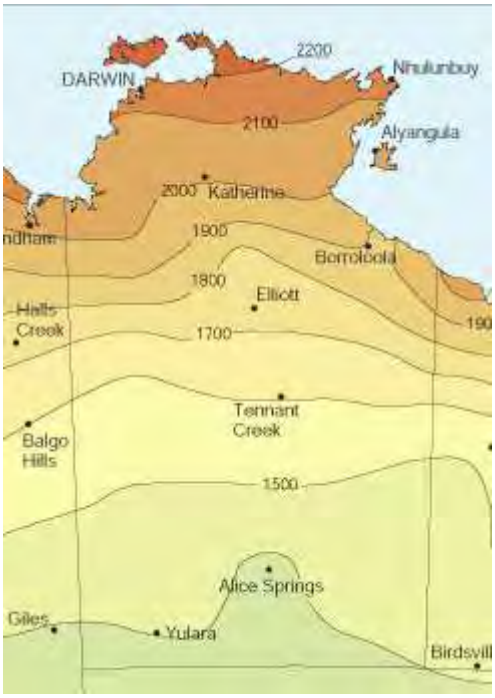

Figure 2 - Evapotranspiration rates in mm per year across the Northern Territory.

3 Simulation Inputs

3.1 Digital Elevation Models

The digital elevation model (DEM) was the same 60 m model used in phase 1 of the project. This was composited from three separate DEM sources: a LIDAR survey, Shuttle Radar Topographic Mission (STRM) data and a bathymetric DEM (Geoscience Australia, 2009). For details on the construction and processing of the input DEM, please refer to the phase 1 report (Saunders et al., 2014). A small refinement was made to the river depths in the South Alligator river in this phase, which had previously been taken from the bathymetric DEM. The depth of the river was reconstructed based on transects carried out by Woodroffe et al. (1986). Where the transects did not cross the river system the depth of the river was estimated from paleochannels in the transects. This correction resulted in lower river depths than used in the previous DEM.

3.2 Tidal Boundary Forcing

Due to the lack of available data in the Van Diemen Gulf, tidal records from Darwin were used for the tidal input, Fig. 3. These tides were scaled to match present day observations of maximum tidal inundation in the downstream region around Boggy plain. Tidal time series from March and October 2012 were used in the model. Additionally, a tidal time series incorporating a 3 m storm surge event was used, shown in Fig. 4. The value of 3 m was estimated as a plausible worst-case scenario, occurring at the peak of the tidal cycle. The estimation was based on storm surges recorded in Darwin (2 m for cyclone Tracey, 1974) and areas surrounding the gulf (5-6 m for cyclone Monica, 2006, in Junction Bay, ‘several meters’ for cyclone Ingrid, 2005, at Drysdale Island).

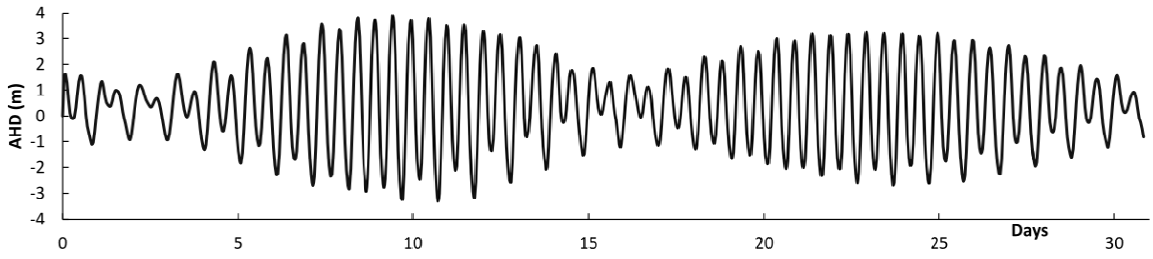

Figure 3 - Darwin March 2012 tide

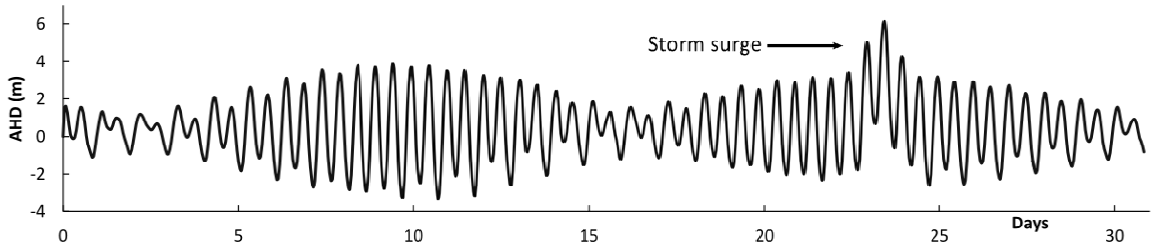

Figure 4 - Darwin March 2012 tide with storm surge event

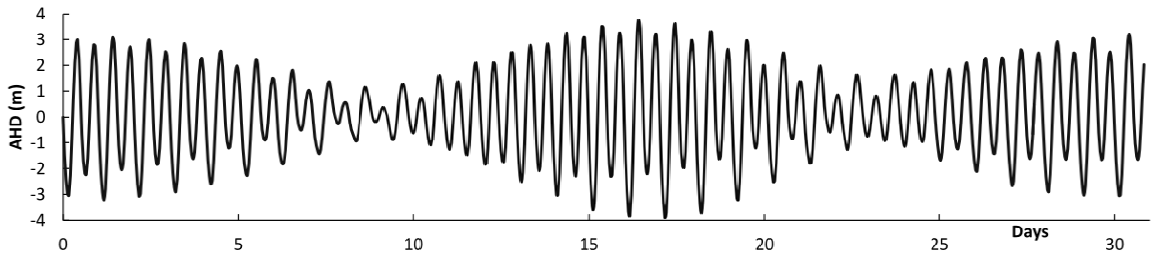

Figure 5 - Darwin October 2012 tide

3.3 Salinity model

The salinity model required a starting condition for the initial salinity distribution. No spatial large-scale salinity data was available over the modelled region to use for these conditions. However, salinity values have been measured within the South Alligator river system (Woodroffe et al., 1986). The peak dry season values given by Woodroffe et al. (1986) were used for the initial conditions for the October simulation, which started at sea level salinity (36 ppt) at the mouth of the South Alligator, falling to approximately 26 ppt 80 km from the mouth. The same salinity decrease as a function of distance from the mouth was assumed to hold for the East and West Alligator river systems. The initial salinity distribution for the October scenarios is shown in Fig. 6 (left). For the

wet season (March), it was assumed that the river was entirely freshwater. The offshore distribution was not known and was assumed to linearly rise with distance from the shore to the mean sea salinity value of 36 ppt. The initial salinity distribution for the March scenarios is shown in Fig. 6 (right).

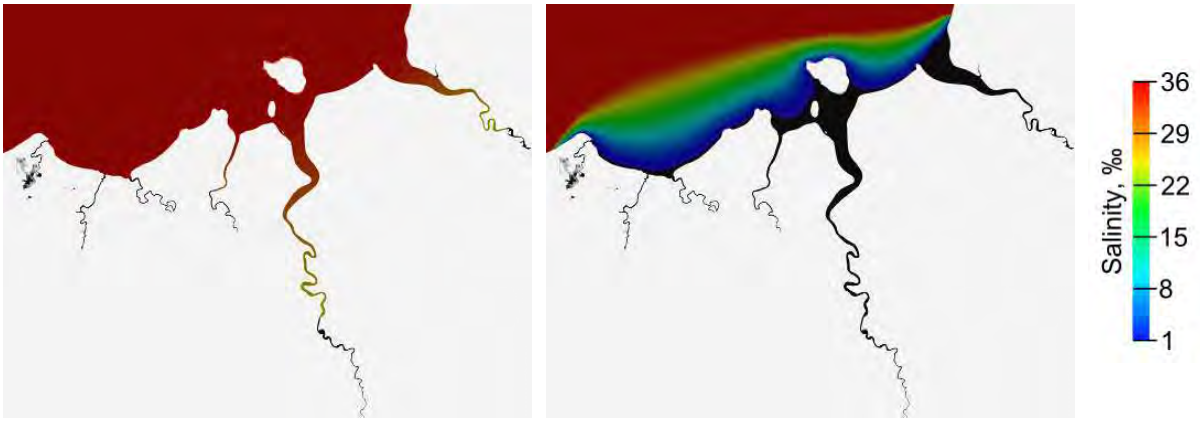

Figure 6 - Initial salinity condition for March (left) and October (right) scenarios

3.4 Scenarios

The scenarios considered are summarised in table 1 below:

No	Month	Sea level	Storm surge	Rainfall
1	March	present day	None	5mm per day
2	March	present day	3 m	5 mm per day, 100 mm over 2 days during storm
3	March	+ 70 cm	None	5mm per day
4	March	+ 70 cm	3 m	5 mm per day, 100 mm over 2 days during storm
5	October	present day	None	None
6	October	+ 70 cm	None	None

Table 1- Scenario conditions for all cases considered

4 Validation

Validation of the salinity component was carried out using comparison to measured data reported by Woodroffe et al. (1986). Further validation, including onshore salinity levels, are currently being carried out using newer data recently gathered from the region. There is strong dependence for salinity on both rainfall, tidal cycles and existing saline deposits making comparison to measured data difficult. Data given by Woodroffe et al. (1986) shows the increase in salinity over time during the dry season since the 'last flood peak in wet season'. To replicate this event, we assumed that the river was entirely freshwater from the flood event and became saline at the mouth of the river. The model was run for seven days and compared to the observed salinity measured by Woodroffe for the same period. The initial conditions for the simulation are shown in Fig. 7 (inset) and the comparison of the results are shown in the main figure. The simulation results are shown as 3 hour averages, with one standard deviation shown as vertical error bars. No bounds on the measured data ranges were given.

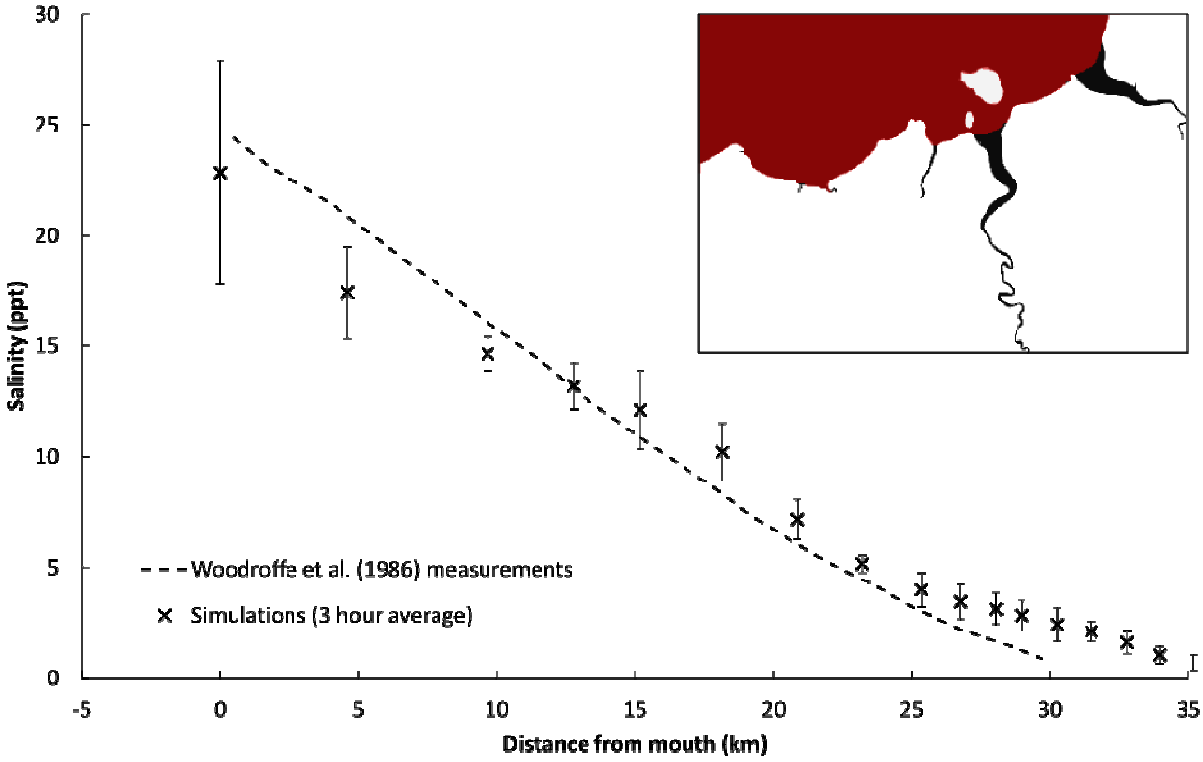

Figure 7 - Validation of the salinity model against observed data; Inset: initial conditions for the simulation

The simulation results give a good match to the observed data ranges and trend.

5 Results

Results from the simulations are shown in the following sections. For the purposes of assessing environment impact the maximum water heights and salinity values over each month are given. These give the worst-case areal extents of inundation due to sea level rise or storm surge, and the corresponding saltwater intrusion. These maximum values do not give a complete picture, however, as they may persist for only a short period of time (especially in the case of a storm surge). To show the baseline trend the median values over each month are also given. The relative difference between the median and maximum values can be used to gauge the overall trend of the inundation conditions. Temporal trends are also shown using percentages of time the water level or salinity is over a threshold value.

5.1 Maximum water levels

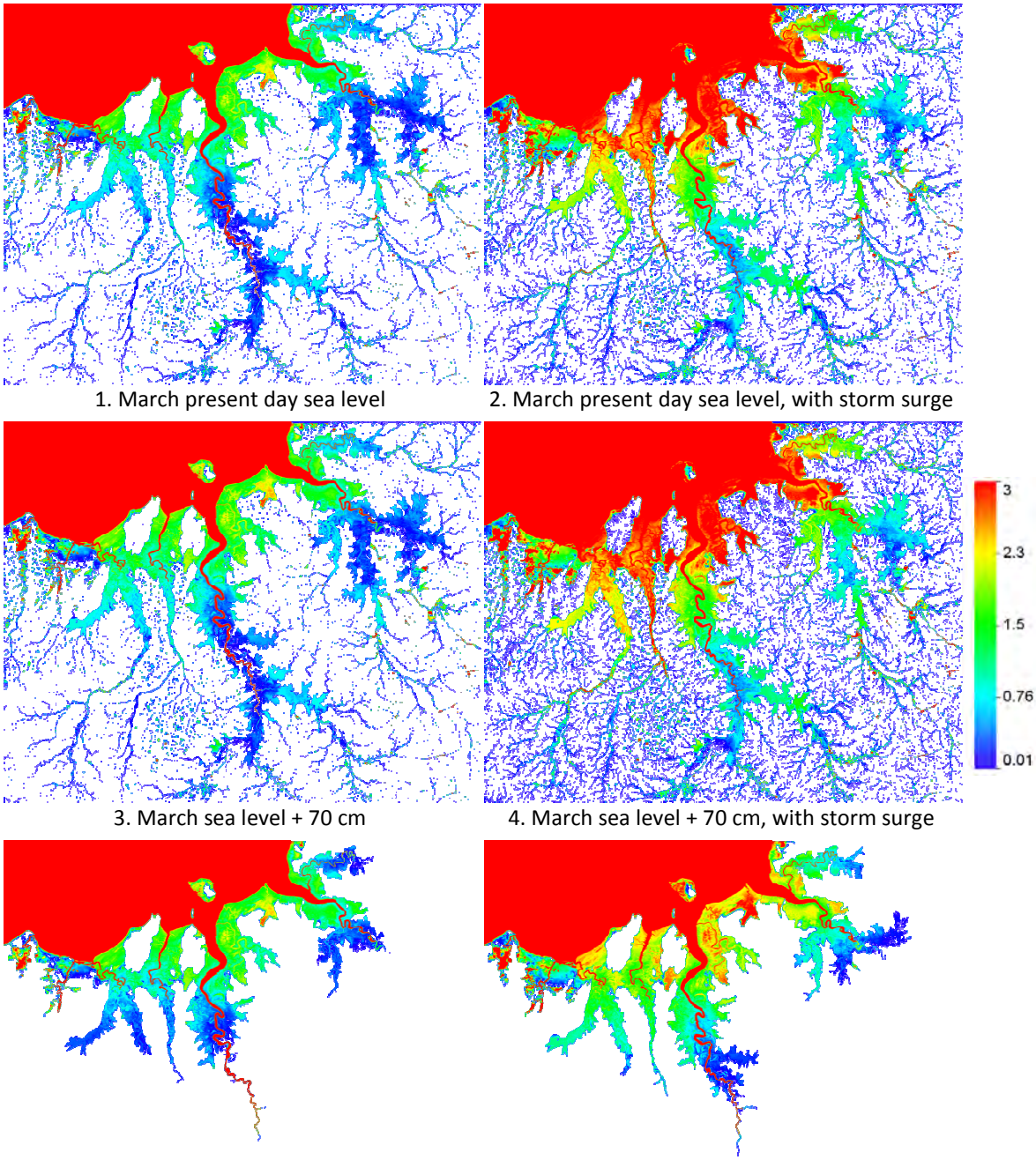

Figure 8 - Maximum water levels (m) and inundation extents

Maximum water levels are shown in Fig. 8 for all scenarios. Note that rainfall is used in the March simulations and the water levels in the catchment network are therefore shown. Storm surge events can be seen to have much higher inundation levels near the coastline. As with phase 1, the boggy plain region is found to flood for the increased sea level scenarios.

5.2 Median water levels

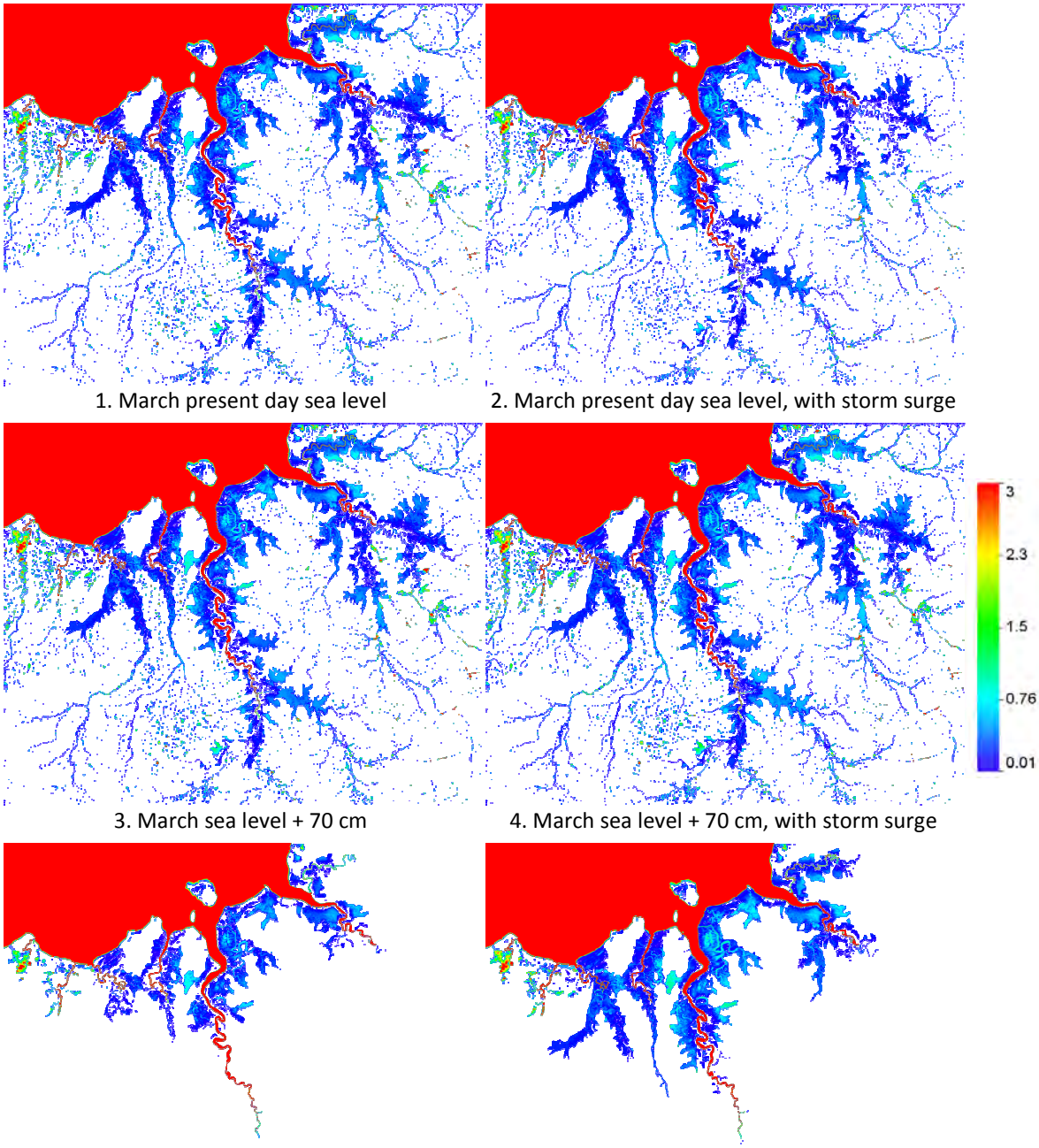

Figure 9 - Median water levels (m)

Median water levels are shown in Fig. 9 for all scenarios. It can be seen that there is are negligible differences between the scenarios with and without with storm surges, showing that the maximum inundation shown in Fig. 8 is a rapid temporal event. However, median upstream water levels for all river systems are much higher for the sea level rise scenarios.

5.3 Inundation frequency

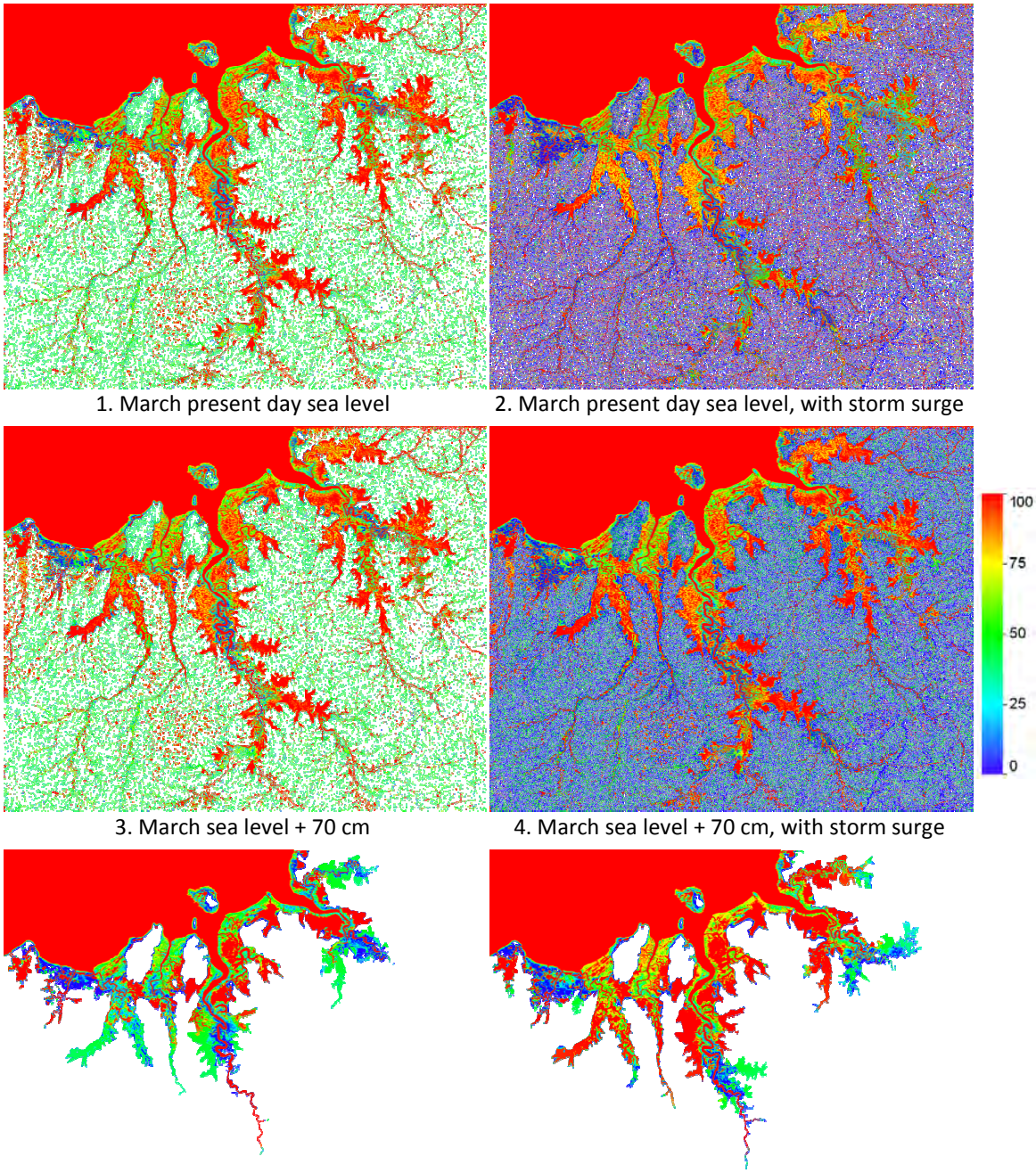

1. March present day sea level
2. March present day sea level, with storm surge
3. March sea level + 70 cm
4. March sea level + 70 cm, with storm surge
5. October present day sea level
6. October sea level + 70 cm

Figure 10 – Inundation frequency (%)

The percentage of time a region has a water level over 1 mm is shown in Fig. 10. Again, there are negligible differences between the scenarios with and without storm surges. The frequency of inundation in the dry season (October) scenarios is found to increase from 50% for the present day to 100% in upstream regions for all river system.

5.4 Maximum salinity levels

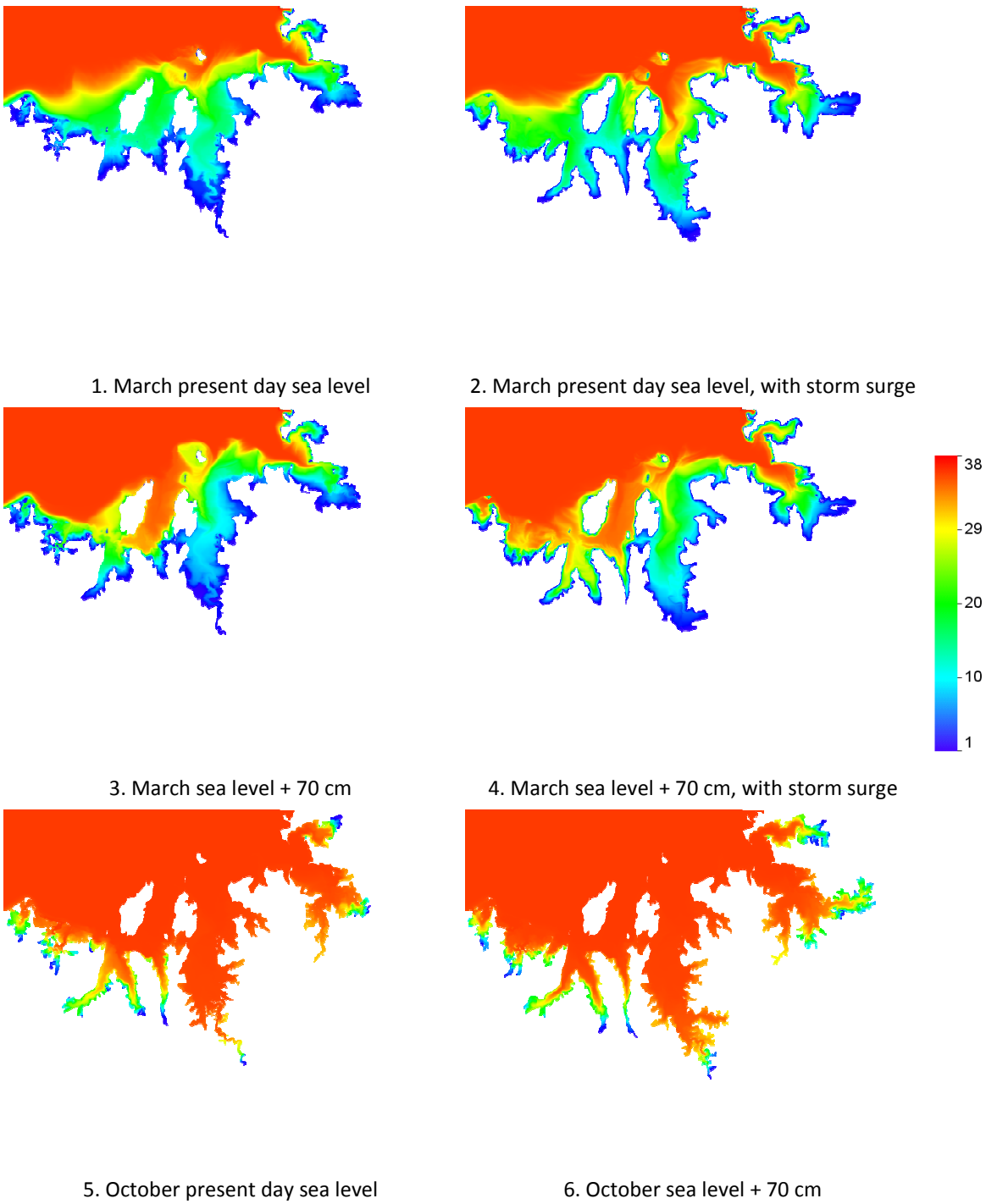

Figure 11 - Maximum salinity levels (ppt)

Maximum salinity levels are shown in Fig. 11 for all scenarios. The storm surge can be seen to have a strong effect on the saltwater intrusion, giving greater areal coverage and increasing the salinity in the upstream regions. Likewise, an increase in the maximum salinity coverage is found in the sea level rise scenarios.

5.5 Median salinity levels

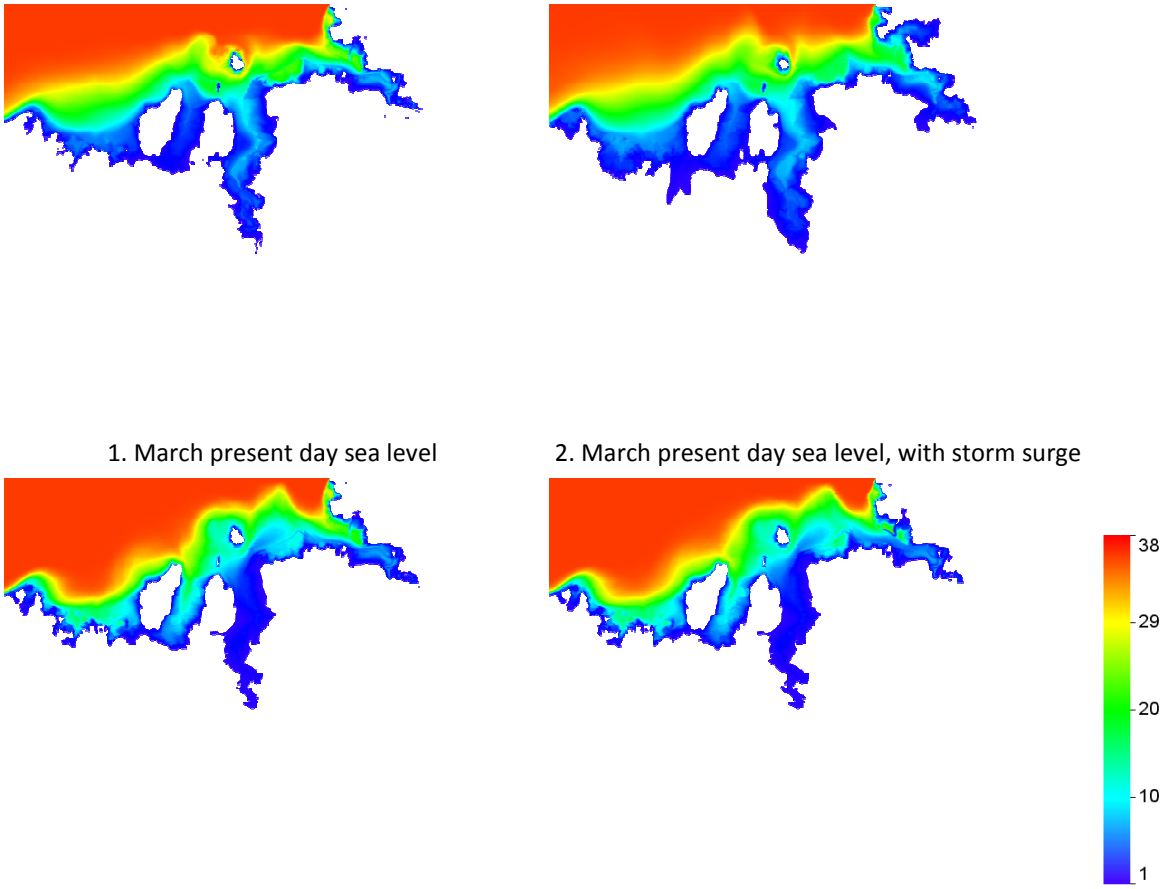

Figure 12 - Median water levels (m)

Median salinity levels are shown in Fig. 12 for all scenarios. Unlike the median water levels, the area affected by saltwater instruction increases during storm surges. The mechanism for this is saltwater being driven onto land during the surge and evaporating, leaving saline deposits. The sea level rise scenarios also show an increase in the areas affected by saltwater intrusion.

5.6 Salinity threshold

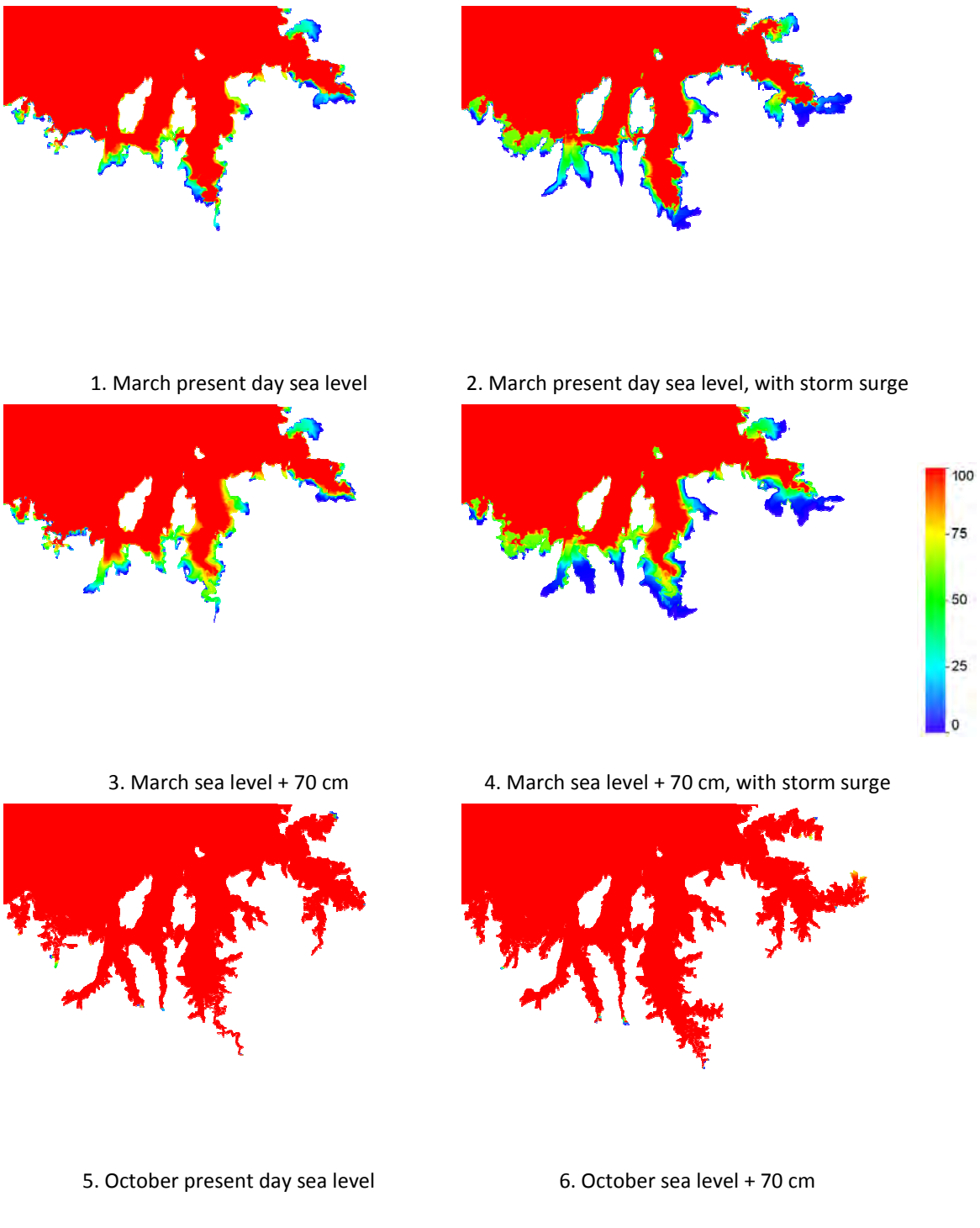

Figure 13 – Percentage time over threshold salinity of 2 ppt (%)

The percentage of time a region has salinity above 2 ppt is shown Fig. 13. This threshold was chosen based on the salinity tolerance of many freshwater plants in the region. As with the median values, storm surge increases the area where the salinity is over this threshold value. The sea level rise scenarios show a similar trend.

5.7 Dynamic flushing of saltwater in Boggy Plain

The upstream area of Boggy Plain, adjacent to the South Alligator river, is a site of special interest due to significance to traditional owners and the large freshwater habitat which serves as a refuge for waterbirds during the dry season. This area was investigated in detail in phase 1, and it was of interest whether this area would be subject to saltwater intrusion during storm surge events.

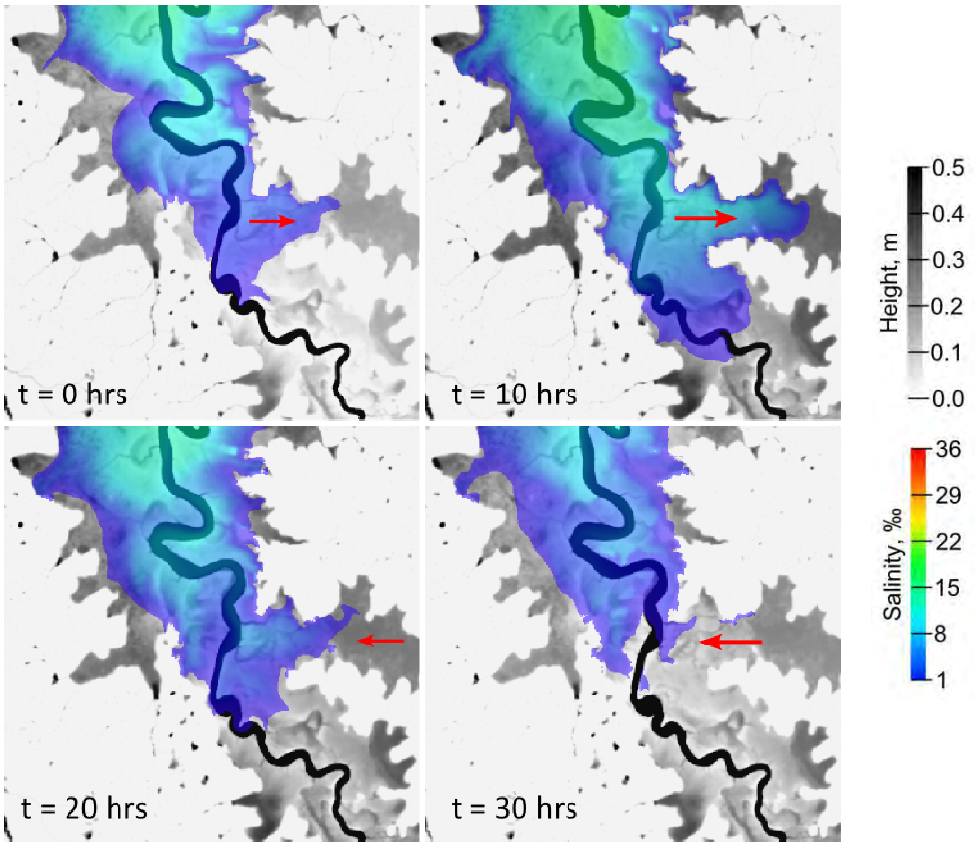

Figure 14 - Saltwater flushing at the entrance to Boggy Plain

Results from the study for the March present day case with a storm surge (scenario 2) are shown in Fig. 14. Water level is shaded from white (dry) to black and the salinity (in parts per thousand) is overlaid in colour. The system showed dynamic behaviour due to the interaction between the transport from the storm surge and the associated heavy rainfall event. The initial effect of the storm surge was to transport saltwater up the South Alligator river and into Boggy plain (Fig. 14, top). However, the heavy rainfall event caused high volumes of water in the catchment which drained into Boggy Plain around 20 hours later, reversing the flow and flushing the saltwater back into the river. Saltwater intrusion into this region is therefore a balance of these effects and will depend on both the severity of the storm surge and any associated rainfall event.

6 Conclusion

We have carried out coupled hydrodynamic and salinity transport modelling for several scenarios in Kakadu National Park. These were used to gauge saltwater intrusion for storm surges and sea level rise in the wet (March) and dry (October) seasons. The model gave a good match to salinity values measured in the South Alligator river. The results for maximum inundation extents match results of phase 1, with upstream areas in all major river systems affected by potential sea level rise. Storm surges were found, as expected, to cause greater inundation along coastal areas and in downstream regions of all the major rivers but to have marginal effects on long term inundation levels. However, storm surges were found to have a significant long term effect on median salinity levels in downstream areas, as saltwater was transported overland during the storm surge and remained as the water evaporated. Sea level rise was also found to cause significant saltwater intrusion into upstream regions of all the major river systems. The saltwater intrusion in some regions was found, though, to be dynamic and dependent on a balance of transport from saline regions and flushing from rainwater. Future work may be necessary to investigate this dynamic process in more detail.

References

BAYLISS, B., BRENNAN, K., ELIOT, I., FINLAYSON, M., HALL, R., HOUSE, T., PIDGOEN, B., WALDEN, D. & WATERMAN, P. 1997. Vulnerability assessment of predicted climate change and sea level rise in the Alligator Rivers Region, Northern Territory Australia. Canberra.

BEGNUDELLI, L., SANDERS, B., 2007, Conservative Wetting and Drying Methodology for Quadrilateral Grid Finite-Volume Models, J. Hydralic Eng. 133, 312-322

CEA, L., PUERTAS, J., M., VAZQUEZ-CENDON, M-E., 2007, Depth Averaged Modelling of Turbulent Shallow Water Flow with Wet-Dry Fronts, Arch Comput Methods Eng, 14, 303–341

GEOSCIENCE AUSTRALIA 2009. Australian bathymetry and topography grid.

GROSS, E. S., KOSE, J. R., AND MONISMITH, S. G., 1999, Evaluation of Advective Schemes for Estuarine Salinity Simulations, Journal of Hydraulic Engineering, 125, 32–46

KNIGHTON, A. D., WOODROFFE, C. D. AND MILLS, K., 1992, The Evolution of Tidal Creek Networks, Mary River, Northern Australia, Earth Surf. Process. Landforms, 17, 167–190

KURGANOV, A., PETROVA, G., 2007, A Second-Order Well-Balanced Positivity Preserving Central-Upwind Scheme for the Saint-Venant System, Commun. Math. Sci., 5, 133-160

SAUNDERS, K., WOOLARD, F. AND PRAKASH M., 2014, Hyrdodynamic modelling of tidal inundation from sea level rise in Kakadu National Park., CSIRO Tech. Report, EP14519, 36 pages, Jan 2014

SAYNOR, M., 2004, Saltwater Intrusion - a Natural Process, Supervising Scientist Note series

SMITH, M., ALLEN, R., MONTEITH, J. L., PERRIER, A., SANTOS PEREIRA, L., SEGEREN, A., 1992, Expert Consultation on Revision of FAO Methodologies for Crop Water Requirements, Rome (Italy),28-31 May 1990 / FAO, Rome (Italy), Land and Water Development Div. , 63

WINN, K. O., SAYNOR, M. J., ELIOT, M. J. & ELIO, I. 2006. Saltwater Intrusion and Morphological Change at the Mouth of the East Alligator River, Northern Territory. Journal of Coastal Research, 137-149.

WOODROFFE, C. D., CHAPPELL, J. M. A., THOM, B. G., WALLENSKY, E., 1986, Geomorphological Dynamics and Evolution of the South Alligator Tidal River and Plains, Northern Territory, Darwin, ANU NARU Mangrove Monograph No. 3

WORLD HERITAGE CONVENTION UNESCO. 2014. Kakadu National Park [Online]. http://whc.unesco.org/en/list/147: UNESCO,. [Accessed 01/12/2013 2013].

CONTACT US

t 1300 363 400
+61 3 9545 2176

e enquiries@csiro.au

w www.csiro.au

YOUR CSIRO

Australia is founding its future on science and innovation. Its national science agency, CSIRO, is a powerhouse of ideas, technologies and skills for building prosperity, growth, health and sustainability. It serves governments, industries, business and communities across the nation.

FOR FURTHER INFORMATION

Computation Informatics

James Hilton

t +61 3 9545 8002

e James.Hilton@csiro.au

w www.csiro.au/Outcomes/Environment/Australian-Landscapes-geophysical-modelling.aspx

Computational Informatics

Mahesh Prakash

t +61 3 9545 8010

e Mahesh.Prakash@csiro.au

w www.csiro.au/Outcomes/Environment/Australian-Landscapes-geophysical-modelling.aspx

Marine and Atmospheric Research

Peter Bayliss

t +61 7 3833 5905

e Peter.Bayliss@csiro.au